

AIMS on Applied Mathematics **Vol. 10**

Hyperbolic Problems: Theory, Numerics, Applications

**Alberto Bressan
Marta Lewicka
Dehua Wang
Yuxi Zheng
Editors**



American Institute of Mathematical Sciences

EDITORIAL COMMITTEE

Editor in Chief: Monique Chyba (USA), Benedetto Piccoli (USA)

Members: José Antonio Carrillo de la Plata (UK), Mickael Chekroun (USA),
Alessio Figalli (USA), Kenneth Karlsen (Norway),
James Keener (USA), Yannick Privat (France),
Gilles Vilmart (Switzerland), Thaleia Zariphopoulou (UK).

AMS 2010 Classifications: Primary: 35-06; Secondary: 35L65, 35L67, 35Q35,
65-06, 76-06

ISBN-10: 1-60133-023-5; ISBN-13: 978-1-60133-023-9

© 2020 by the American Institute of Mathematical Sciences. All rights reserved. This work may not be translated or copied in whole or part without the written permission of the publisher (AIMS, LLC, P.O. Box 2604, Springfield, MO 65801-2604, USA), except for brief excerpts in connection with reviews or scholarly analysis. Use in connection with any form of information storage and retrieval, electronic adaptation, computer software, or by similar or dissimilar methodology now known or hereafter developed is forbidden. The use in this publication of trade names, trademarks, service marks, and similar terms, even if they are not identified as such, is not to be taken as an expression of opinion as to whether or not they are subject to proprietary rights.

aimsciences.org

MODELLING, NUMERICAL METHOD AND ANALYSIS OF THE COLLAPSE OF CYLINDRICAL SUBMARINES GRANULAR MASS

E.D. FERNÁNDEZ-NIETO

Departamento de Matemática Aplicada I, Universidad de Sevilla. E.T.S. Arquitectura,
Avda, Reina Mercedes, s/n. 41012 Sevilla, Spain.

MANUEL J. CASTRO

Departamento de Análisis Matemático, Universidad de Málaga,
F. Matemáticas, Campus Teatinos S/N, Spain.

ANNE MANGENEY

Equipe de Sismologie, IGP, 4, pl. Jussieu 75232, Paris cedex 05, France.

ABSTRACT. In this work we focus on the numerical study of shallow submarine avalanches. Submarine avalanches could be modeled by a two-layer shallow-water Savage-Hutter type model (see [9]). The system is discretized by a finite volume solver named as IFCPH, that results from a combination of IFCP solver (see [11]) and the standard HLL solver (see [13]). Concerning the applications, we focus on the collapse of an initially cylindrical submarine granular mass along an horizontal plane. It is well established by laboratory studies ([14]) and the dimensional analysis of the Savage-Hutter model and numerical simulations ([16]), that the final profile of the landslide depends on the aspect ratio $a = H_i/R_i$, where H_i and R_i are the initial height and radius, respectively, and the effective friction angle. In this work, a similar behavior, for the two-layer model, and the final profile of the landslide only depends on the two aspect ratios: $a_H = H_1/H_2$ and $a_2 = H_2/R$, with R and H_2 the initial radius and height of the sediment column, respectively, and H_1 the initial height of the water above the sediment column. The sensitivity of the granular dynamics and of the associated water perturbation to these two aspect ratios is investigated.

1. Introduction. Submarine avalanches may occur when a sediment layer lying on the ocean bottom suddenly becomes unstable. These avalanches may generate tsunami waves that carry the signature of their characteristics and dynamics. These processes are however difficult to simulate because of the complex interaction between the granular and the fluid phases [2] and because of the accurate derivation of the shallow approximation for both the sediment and fluid layers. In [9] a two-layer Shallow Water Equation (SWE) system has been proposed to simulate submarine avalanches and the potentially generated tsunami waves. The first layer corresponds to the fluid and the second one to the sediment layer.

2000 *Mathematics Subject Classification.* Primary: 35L45, 35L65, 65Z05; Secondary: 65M99.

Key words and phrases. Submarine Avalanches, Bilayer Shallow Water, Well-Balanced, Finite Volume Method.

This research has been partially supported by the Spanish Government under grants MTM 2015-70490-C2-1-R and MTM 2015-70490-C2-2-R with the participation of FEDER, by the ANR contract ANR-11-BS01-0016 LANDQUAKES, the USPC PEGES project and the ERC contract ERC-CG-2013-PE10-617472 SLIDEQUAKES.

* Corresponding author: Enrique D. Fernández-Nieto.

For the sediment layer, a Savage-Hutter type model is considered. The pioneering work of Savage-Hutter [24] derives a model to describe granular flows over a sloping plane based on a Coulomb friction law that describes the avalanche/bottom interaction.

One of the characteristics of the model proposed in [9] is that the definition of the Coulomb friction term takes into account buoyancy effects involved in submarine avalanches. Another characteristic is that, depending on the ratio between the water density and the sediment density, the motion of the sediment avalanche can be more or less influenced by the presence of the fluid.

In this work we present a two-dimensional two-layer model that is a generalization of the 1D model presented in [9] in cartesian coordinates. One of the questions arising in the deduction of the model is the choice of the coordinate system in which the model is deduced. Let us remember that the Saint-Venant equations are set up in cartesian coordinates, but it is valid only for almost flat topography, thus not relevant for debris avalanches in particular. On the other hand, the Savage-Hutter model uses the curvilinear coordinate along a sloping plane. New Savage-Hutter models over a general bottom have been proposed by Bouchut et al. in [1], taking into account the curvature of the topography. In [3], Bouchut and Westdickenberg generalize the previous models for small or for general slope variation in two dimensions. The 1D model introduced in [9] for submarine avalanches has been also deduced on local coordinate along the topography, by taking into account the curvature of the bottom. Here, we only focus on the spreading of an initially cylindrical submarine granular mass on a flat bottom, therefore, cartesian coordinates could be used. The resulting model has non-conservative terms, that come from the pressure terms, and can be written under the general formulation

$$\frac{\partial W}{\partial t} + \frac{\partial F_1}{\partial x_1}(W) + \frac{\partial F_2}{\partial x_2}(W) + B_1(W) \frac{\partial W}{\partial x_1} + B_2(W) \frac{\partial W}{\partial x_2} = S(W), \quad (1)$$

where the unknown $W(\mathbf{x}, t)$ is defined in the domain $D \times (0, T)$, where D is a subset of \mathbb{R}^2 , with values in an open subset Ω of \mathbb{R}^N ; F_i , $i = 1, 2$ are regular functions from Ω to \mathbb{R}^N ; B_i , $i = 1, 2$ are regular function matrices from Ω to $\mathcal{M}_{N \times N}(\mathbb{R})$ and S , is defined from Ω to \mathbb{R}^N .

Finite volume path-conservative schemes ([19]) are well-adapted to approximate non-conservative hyperbolic system (1). Here, we propose to combine two particular path-conservative schemes: the IFCP solver (Intermediate Field Capturing Parabola method, see [11]), that is very well-adapted to approximate two-layer shallow-water type systems, with the robust extension of HLL solver to the non-conservative framework (see [6]). IFCP solver provides accurate results, similar to the standard path-conservative Roe scheme ([20]), being IFCP more efficient, from the computational point of view, but may present disturbances in wet/dry fronts, while HLL solver is more robust in such situations. Therefore, the main objective is to naturally combine both solvers, and this can be easily done in the framework of PVM schemes. Both solvers, IFCP and HLL could be re-written as PVM methods with a similar structure, that allows to combine them in a very natural way, obtaining the IFCPH solver.

As the two-dimensional landslide model is rotationally invariant, IFCPH solver could be extended as the HLL solver to deal with the contact discontinuities associated to the tangential velocities (see [26])

This work is organized as follows. In Section 2 we present a 2D extension of the model proposed in [9] for submarine avalanches. Section 3 is devoted to the presentation of the IFCPH finite volume solver. Finally, in Section 4, we analyze the dependency of the model on the parameters involved both in terms of avalanche dynamics and water wave generation.

2. 2D two-layer Submarine landslide model. In [9] a two-layer 1D model is presented to study submarine avalanches. The first layer corresponds to the water and it is modeled by the standard shallow-water system and the submerged sediment layer is modeled by a Savage-Hutter type system (see [24]).

Savage-Hutter model is characterized by the presence of a Coulomb friction term. This term opposes the avalanche motion and depends on the pressure at the bottom and on a friction coefficient. When the driving forces are higher than a threshold, the avalanche is moving and Coulomb friction applies to the flow [15]. When the driving forces are smaller, the material stops. The Coulomb friction term in the model proposed by [9] also includes the buoyancy effect.

In this section we present a 2D simplified extension of the model proposed in [9] with flat bottom topography. With subindex 1 we denote the unknowns corresponding to the fluid layer: h_1 is the height of the fluid layer and $\vec{q}_1 = (q_{11}, q_{12}) = (h_1 U_1, h_1 V_1)$ is the fluid flux, with $\vec{u}_1 = (U_1, V_1)$ the fluid velocity vector. Index 2 corresponds to the sediment layer: by h_2 we denote the height of the sediment layer and $\vec{q}_2 = (q_{21}, q_{22}) = (h_2 U_2, h_2 V_2)$ is the flux of the granular material, with $\vec{u}_2 = (U_2, V_2)$, the granular velocity vector

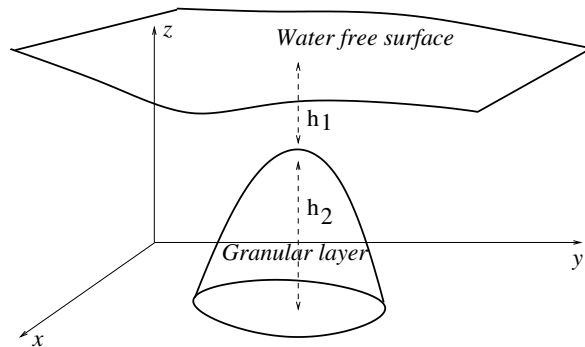


FIGURE 1. Notation: 2D submarine avalanche on a flat bottom

$$\left\{ \begin{array}{l} \partial_t(h_1) + \partial_x(h_1 U_1) + \partial_y(h_1 V_1) = 0, \\ \partial_t(h_1 U_1) + \partial_x(h_1 U_1^2) + \partial_y(h_1 U_1 V_1) + gh_1 \partial_x(h_1 + h_2) = 0 \\ \partial_t(h_1 V_1) + \partial_x(h_1 U_1 V_1) + \partial_y(h_1 V_1^2) + gh_1 \partial_y(h_1 + h_2) = 0 \\ \partial_t(h_2) + \partial_x(h_2 U_2) + \partial_y(h_2 V_2) = 0, \\ \partial_t(h_2 U_2) + \partial_x(h_2 U_2^2) + \partial_y(h_2 U_2 V_2) + gh_2 \partial_x(rh_1 + h_2) = \mathcal{T}_x \\ \partial_t(h_2 V_2) + \partial_x(h_2 U_2 V_2) + \partial_y(h_2 V_2^2) + gh_2 \partial_y(rh_1 + h_2) = \mathcal{T}_y \end{array} \right. \quad (2)$$

where g is the gravity acceleration, $r = \rho_f/\rho_s$ is the ratio between the fluid density, that it is supposed to be $\rho_f = 1000 \text{ kg.m}^{-3}$ and the density of the granular material, ρ_s . Typical values of ρ_s are between 1200 to 2500 kg.m^{-3} depending on the solid volume fraction and on the material involved. Note that we consider here quite dense granular material consistent with our model. As a result, the density ratio is $0.4 < r < 0.8$. $\mathcal{T} = (\mathcal{T}_x, \mathcal{T}_y)$ denotes the Coulomb friction term:

$$\mathcal{T} = -\frac{g(1-r)h_2\mu}{\sqrt{U_2^2 + V_2^2}} \begin{pmatrix} U_2 \\ V_2 \end{pmatrix}.$$

Note that this term is multi-valuated when $|\vec{u}_2| = 0$.

The simplest friction law corresponds to a constant friction coefficient:

$$\mu = \tan(\delta), \quad (3)$$

where δ is the friction angle, although more complex friction terms have been used to simulate natural subaerial or submarine landslides (see [17], [22]). For example, in order to incorporate turbulence effects, McDougall and Hungr [18] proposed to add a turbulent friction term proportional to $(U_2^2 + V_2^2)$. Other definitions, deduced from experimental data, have been proposed by Pouliquen (see [23]) where the friction coefficient depends on the velocity and thickness of the granular layer. This law is widely used in the literature but involves at least three parameters that are difficult to calibrate for natural landslides (see e. g. [4]).

Model (2) can be written in the same form as (1), by setting:

$$W = \begin{pmatrix} h_1 \\ h_1 U_1 \\ h_1 V_1 \\ h_2 \\ h_2 U_2 \\ h_2 V_2 \end{pmatrix}, \quad F_1(W) = \begin{pmatrix} h_1 U_1 \\ h_1 U_1^2 \\ h_1 U_1 V_1 \\ h_2 U_2 \\ h_2 U_2^2 \\ h_2 U_2 V_2 \end{pmatrix}, \quad F_2(W) = \begin{pmatrix} h_1 V_1 \\ h_1 U_1 V_1 \\ h_1 V_1^2 \\ h_2 V_2 \\ h_2 U_2 V_2 \\ h_2 V_2^2 \end{pmatrix},$$

$$B_1(W) = \begin{pmatrix} 0 & 0 & 0 & 0 & 0 & 0 \\ gh_1 & 0 & 0 & gh_1 & 0 & 0 \\ 0 & 0 & 0 & 0 & 0 & 0 \\ 0 & 0 & 0 & 0 & 0 & 0 \\ rgh_2 & 0 & 0 & gh_2 & 0 & 0 \\ 0 & 0 & 0 & 0 & 0 & 0 \end{pmatrix},$$

$$B_2(W) = \begin{pmatrix} 0 & 0 & 0 & 0 & 0 & 0 \\ 0 & 0 & 0 & 0 & 0 & 0 \\ gh_1 & 0 & 0 & gh_1 & 0 & 0 \\ 0 & 0 & 0 & 0 & 0 & 0 \\ 0 & 0 & 0 & 0 & 0 & 0 \\ rgh_2 & 0 & 0 & gh_2 & 0 & 0 \end{pmatrix},$$

$S(W) = S_{1,\mathcal{T}}(W) + S_{2,\mathcal{T}}(W)$ is defined by the Coulomb Friction terms,

$$S_{1,\mathcal{T}}(W) = -\frac{g(1-r)h_2\mu}{\sqrt{U_2^2 + V_2^2}} \begin{pmatrix} 0 \\ 0 \\ U_2 \\ 0 \end{pmatrix}, \quad S_{2,\mathcal{T}}(W) = -\frac{g(1-r)h_2\mu}{\sqrt{U_2^2 + V_2^2}} \begin{pmatrix} 0 \\ 0 \\ 0 \\ V_2 \end{pmatrix}.$$

Note that $F_i(W)$, $i = 1, 2$ represent the convective terms and $B_i(W)\partial_x W$ are the pressure terms.

System (2) is rotationally invariant. Thus, if we denote by $\eta = (\eta_1, \eta_2)$ an unit vector, and

$$R_\eta = \begin{pmatrix} \eta_1 & \eta_2 \\ -\eta_2 & \eta_1 \end{pmatrix}, \quad T_\eta = \left(\begin{array}{cc|cc} 1 & 0 & 0 & 0 \\ 0 & R_\eta & 0 & 0 \\ \hline 0 & 0 & 1 & 0 \\ 0 & 0 & 0 & R_\eta \end{array} \right).$$

and if we also denote

$$F_\eta(W) = F_1(W)\eta_1 + F_2(W)\eta_2, \quad B_\eta(W, \mathbf{s}) = B_1(W)\eta_1 + B_2(W)\eta_2, \\ S_\eta(W) = S_{1,\mathcal{T}}(W)\eta_1 + S_{2,\mathcal{T}}(W)\eta_2.$$

Then, the following properties follows:

$$T_\eta F_\eta(W) = F_1(T_\eta W), \quad T_\eta B_\eta(W) = B_1(T_\eta W) \text{ and } T_\eta S_\eta(W) = S_{1,\mathcal{T}}(T_\eta W). \quad (4)$$

Moreover, for any unit vector η , system (2) can be rewritten as follows:

$$\partial_t W + \partial_\eta F_\eta + \partial_{\eta^\perp} F_{\eta^\perp} + B_\eta(W)\partial_\eta W + B_{\eta^\perp}(W)\partial_{\eta^\perp} W = S_\eta(W) + S_{\eta^\perp}(W).$$

Multiplying previous system by T_η and using (4) we obtain

$$\partial_t(T_\eta W) + \partial_\eta F_1(T_\eta W) + B_1(T_\eta W)\partial_\eta T_\eta W = S_1(T_\eta W) + \mathcal{R}_{\eta^\perp} \quad (5)$$

where

$$\mathcal{R}_{\eta^\perp} = -T_\eta \left(\partial_{\eta^\perp} F_{\eta^\perp} + B_{\eta^\perp}(W)\partial_{\eta^\perp} W - S_{\eta^\perp}(W) \right).$$

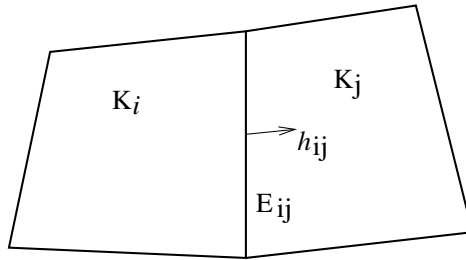


FIGURE 2. Notation, control volumes

Up to our knowledge, there is not in the bibliography results on the existence and uniqueness of solution of this model. It can be seen as a bilayer Shallow Water system with a specific definition of the friction terms. In this sense we can remark that in [25] an existence theorem of global weak solutions is presented for a bilayer Shallow Water system with other friction terms and capillary effects.

3. Numerical scheme. First we set a partition of the domain Ω into control volumes. We denote the volumes that define the mesh by K_i . Here, quadrilateral finite volume meshes are considered. In any case, the description of the numerical scheme is also valid for arbitrary meshes. Let also denote by $|K_i|$ the area of the volume K_i and by E_{ij} the common edge between the volumes K_i and K_j . d_{ij} is the distance between the center of mass of both volumes, and η_{ij} is the unitary normal vector to E_{ij} outward to K_i (see Figure 2). We will also denote by W_i^n the approximation computed by the numerical scheme of the cell average of the solution at every volume K_i at time t^n :

$$W_i^n \approx \frac{1}{|K_i|} \int_{K_i} W(x, t^n) dx.$$

Here a two step method is used to discretize (2). In the first step, the Coulomb friction term is neglected and the non-conservative hyperbolic system is discretized by means of the IFCPH path-conservative finite volume solver, to obtain the value $W_i^{n+1/2}$ given by:

$$W_i^{n+1/2} = W_i^n - \frac{\Delta t}{|K_i|} \sum_{j \in K_i} |E_{ij}| \mathcal{D}^-(W_i^n, W_j^n, \eta_{ij}). \quad (6)$$

In the second step, that corresponds to the discretization of the Coulomb friction term, we obtain W_i^{n+1} from $W_i^{n+1/2}$ as follows:

We set $h_{1,i}^{n+1} = h_{1,i}^{n+1/2}$, $\bar{q}_{1,i}^{n+1} = \bar{q}_{1,i}^{n+1/2}$ and $h_{2,i}^{n+1} = h_{2,i}^{n+1/2}$. In order to compute $\bar{q}_{2,i}^{n+1}$, let us first define $\bar{u}_{2,i}^*$ as follows,

$$\bar{u}_{2,i}^* = \bar{u}_{2,i}^{n+1/2} - \Delta t \frac{g(1-r)\mu}{|u_{2,i}^{n+1/2}|} \bar{u}_{2,i}^{n+1/2}.$$

Then we proceed as follows: if $|\bar{u}_{2,i}^*| \leq g(1-r)\mu$ then we set $\bar{u}_{2,i}^{n+1} = \bar{u}_{2,i}^*$. Otherwise $\bar{u}_{2,i}^{n+1} = 0$. Finally, $\bar{q}_{2,i}^{n+1}$ is obtained multiplying $\bar{u}_{2,i}^{n+1}$ by $h_{2,i}^{n+1}$.

In order to define $\mathcal{D}^-(W_i^n, W_j^n, \eta_{ij})$, we consider at each edge E_{ij} of the finite volume mesh the following 1D projected Riemann problem (see [5], [7] and [10]):

$$\begin{cases} \partial_t W + \partial_{\eta_{ij}} F_\eta + B_{\eta_{ij}}(W) \partial_{\eta_{ij}} W = 0, \\ W(x, y, t = 0) = \begin{cases} W_i & \text{if } (x, y) \in K_i, \\ W_j & \text{if } (x, y) \in K_j. \end{cases} \end{cases}$$

Notice that taking into account the invariance by rotation property (4)

$$\begin{aligned} & \partial_t W + \partial_{\eta_{ij}} F_\eta + B_{\eta_{ij}}(W) \partial_{\eta_{ij}} W = \\ & = T_{\eta_{ij}}^{-1} \left(\partial_t T_{\eta_{ij}} W + \partial_{\eta_{ij}} F_1(T_{\eta_{ij}} W) + B_1(T_{\eta_{ij}} W) \partial_{\eta_{ij}} T_{\eta_{ij}} W \right). \end{aligned}$$

Then, we propose to define

$$\mathcal{D}^-(W_i^n, W_j^n, \eta_{ij}) = T_{\eta_{ij}}^{-1} \mathcal{D}^-(T_{\eta_{ij}} W_i^n, T_{\eta_{ij}} W_j^n)$$

being $D^-(T_{\eta_{ij}}W_i^n, T_{\eta_{ij}}W_j^n)$ the path-conservative fluctuation associated to the following 1D problem:

$$\begin{cases} \partial_t w(\xi, t) + \partial_\xi F_1(w) + B_1(w)\partial_\xi w = 0, \\ w(\xi, t = 0) = \begin{cases} T_{\eta_{ij}}W_i & \text{if } \xi < 0, \\ T_{\eta_{ij}}W_j & \text{if } \xi > 0. \end{cases} \end{cases} \quad (7)$$

System (7) has non-conservative products. The presence of the nonconservative product implies that the notion of weak solution in the sense of distributions cannot be used. The theory introduced by Dal Maso, LeFloch, and Murat [8] is followed here to define weak solutions of (7). This theory allows one to define the nonconservative product $B_1(w)\partial_\xi w$ as a bounded measure provided a family of Lipschitz continuous paths $\varphi : [0, 1] \times \Omega \times \Omega \rightarrow \Omega$ is prescribed, which must satisfy certain natural regularity conditions. Here, the family of straight segments is considered:

$$\varphi(s; w_L, w_R) = w_L + s(w_R - w_L).$$

Moreover, the chosen path will play also an important role in the discretization of the system. As mentioned before, here path-conservative finite volume framework will be used.

Moreover, system (7) has two linearly degenerated fields associated to the tangential velocities of each layer with respect to the normal vector η_{ij} , that act as two passive scalars. In this way, the definition of $D^-(T_{\eta_{ij}}W_i, T_{\eta_{ij}}W_j)$ is blocked based: the first block corresponds to the non passive scalar unknowns and the second block to the passive scalar unknowns.

To define $D^-(T_{\eta_{ij}}W_i, T_{\eta_{ij}}W_j)$, we introduce the following notation. Let \mathcal{N} denote the set of index associated to the non passive scalar unknowns, that for that (7) is $\mathcal{N} = \{1, 2, 4, 5\}$. We also denote by $[D^-]_{\mathcal{N}}$ the vector defined by the components of D^- with index in \mathcal{N} .

The definition of the numerical scheme is done in the following two steps:

◦ *Step 1:* Definition of $[D^-(w_i, w_j)]_{\mathcal{N}}$.

We consider here path-conservative numerical schemes, corresponding to the following definition:

$$\begin{aligned} [D^-(w_i, w_j)]_{\mathcal{N}} = & \frac{1}{2} \left([F_1(w_j) - F_1(w_i)]_{\mathcal{N}} + B_{1,ij}[w_j - w_i]_{\mathcal{N}} \right. \\ & \left. - Q_{ij}([w_j - w_i]_{\mathcal{N}} + A_{ij}^{-1}[S_{1,\mathcal{T},ij}]_{\mathcal{N}}) \right), \end{aligned} \quad (8)$$

In the previous equation A_{ij} is a generalized Roe matrix (see [20, 19]) associated to (7) for the equations of the set \mathcal{N} , that is

$$A_{ij}[w_j - w_i]_{\mathcal{N}} = [F_1(w_j) - F_1(w_i)]_{\mathcal{N}} + B_{1,ij}[w_j - w_i]_{\mathcal{N}},$$

where

$$B_{1,ij}[w_j - w_i]_{\mathcal{N}} = \int_0^1 [B_1(\varphi(s, w_i, w_j))\partial_s \varphi(s, w_i, w_j)]_{\mathcal{N}} ds$$

and

$$[S_{1,\mathcal{T},ij}]_{\mathcal{N}} = [S_{1,\mathcal{T}}(w_{ij})]_{\mathcal{N}},$$

being w_{ij} an intermediate state computed from w_i and w_j .

Note that the numerical diffusion term $Q_{ij}([w_j - w_i]_{\mathcal{N}} + A_{ij}^{-1}[S_{1,\tau,ij}]_{\mathcal{N}})$ depends on the Coulomb friction term. This correction is critical in order to preserve accurately the stationary solutions of the form:

$$\vec{u}_1 = \vec{0}, \quad \vec{u}_2 = \vec{0}, \quad h_1 + h_2 = cst, \quad \text{and} \quad \partial_x h_2 \leq \mu \partial_y h_2 \leq \mu.$$

The viscosity matrix Q_{ij} is defined by considering the IFCP method (see [11]):

$$Q_{ij} = \alpha_0^{ij} Id + \alpha_1^{ij} A_{ij} + \alpha_2^{ij} A_{ij}^2 \quad (9)$$

where α_l^{ij} , $l = 0, 1, 2$ are defined in terms of the wave speed of the system:

$$\begin{aligned} \alpha_0^{ij} &= \delta_L S_R^{ij} S_{int}^{ij} + \delta_R S_L^{ij} S_{int}^{ij} + \delta_{int} S_L^{ij} S_R^{ij}, \\ \alpha_1^{ij} &= -S_L^{ij}(\delta_R + \delta_{int}) - S_R^{ij}(\delta_L + \delta_{int}) - S_{int}^{ij}(\delta_L + \delta_R), \\ \alpha_2^{ij} &= \delta_L + \delta_R + \delta_{int} \end{aligned} \quad (10)$$

with

$$\begin{aligned} \delta_L &= \frac{|S_L^{ij}|}{(S_L^{ij} - S_R^{ij})(S_L^{ij} - S_{int}^{ij})}, & \delta_R &= \frac{|S_R^{ij}|}{(S_R^{ij} - S_L^{ij})(S_R^{ij} - S_{int}^{ij})}, \\ \delta_{int} &= \frac{|S_{int}^{ij}|}{(S_{int}^{ij} - S_L^{ij})(S_{int}^{ij} - S_R^{ij})}. \end{aligned}$$

Here, S_L^{ij} and S_R^{ij} are approximations of the slowest and fastest waves (respectively) of the Riemann problem associated to intercell E_{ij} . Here, the following expressions are used:

$$S_L^{ij} = \min(\lambda_{ext,i}^-, \lambda_{ext,ij}^-), \quad S_R^{ij} = \max(\lambda_{ext,j}^+, \lambda_{ext,ij}^+).$$

S_{int}^{ij} is defined by

$$S_{int}^{ij} = s_{ij} \max(|\lambda_{int,ij}^-|, |\lambda_{int,ij}^+|) \quad (11)$$

with

$$s_{ij} = \begin{cases} \text{sign}(S_L^{ij}) & \text{if } |S_L^{ij}| \geq |S_R^{ij}|, \\ \text{sign}(S_R^{ij}) & \text{otherwise.} \end{cases} \quad (12)$$

where $\lambda_{ext,i}^- < \lambda_{int,ij}^- < \lambda_{int,ij}^+ < \lambda_{ext,j}^+$ are the eigenvalues of A_{ij} . Moreover, for the case of wet/dry fronts, that is if $h_{k,i}$ or $h_{k,j}$ is zero for $k = 1, 2$, we consider the following definition of the coefficients α_l^{ij} , $l = 0, 1, 2$:

$$\alpha_0^{ij} = \frac{S_R^{ij}|S_L^{ij}| - S_L^{ij}|S_R^{ij}|}{S_R^{ij} - S_L^{ij}}, \quad \alpha_1^{ij} = \frac{|S_R^{ij}| - |S_L^{ij}|}{S_R^{ij} - S_L^{ij}}, \quad \alpha_2^{ij} = 0.$$

With this choice, it is straightforward to check that the Riemann solver reduces to HLL solver (see [6]), which is more robust when wet/dry fronts appear.

Therefore, the resulting numerical scheme reduces to HLL solver in wet/dry areas and in other case reduces to IFCP solver.

◦ *Step 2:* In this second step, we define the components of the numerical fluctuation, D^- , corresponding to the passive scalar unknowns. In this particular system, they correspond to equations 3 and 6. Taking into account the relation between the passive scalar and the other variables, and that their associated wave speeds only depends on the normal velocities of both layers, we propose the following definition:

$$[D^-(w_i, w_j)]_3 = \left([D^-(w_i, w_j)]_1 + [F_1(w_i)]_1 \right) \mathcal{C}_{1,\eta_{ij}^\perp}^* - [F_1(w_i)]_3$$

$$[D^-(w_i, w_j)]_6 = \left([D^-(w_i, w_j)]_4 + [F_1(w_i)]_4 \right) \mathcal{C}_{2, \eta_{ij}^\perp}^* - [F_1(w_i)]_6.$$

where, $\mathcal{C}_{l, \eta_{ij}^\perp}^*$, $l = 1, 2$ is an uncentered approximation of the tangential velocities of each layer through edges E_{ij} :

$$\mathcal{C}_{1, \eta_{ij}^\perp}^* = \begin{cases} [T_{\eta_{ij}} W_i]_3 / h_{1,i} & \text{if } S_{1,ij}^* < 0, \\ [T_{\eta_{ij}} W_j]_3 / h_{1,j} & \text{if } S_{1,ij}^* > 0, \end{cases} \quad \mathcal{C}_{2, \eta_{ij}^\perp}^* = \begin{cases} [T_{\eta_{ij}} W_i]_6 / h_{2,i} & \text{if } S_{2,ij}^* < 0, \\ [T_{\eta_{ij}} W_j]_6 / h_{2,i} & \text{if } S_{2,ij}^* > 0, \end{cases} \quad (13)$$

The values $S_{l,ij}^*$, $l = 1, 2$ are an approximation of the normal velocities through edges E_{ij} . We can use for example $S_{1,ij}^* = ([D^-(w_i, w_j)]_1 + [F_1(w_i)]_1) / h_{1,ij}$ and $S_{2,ij}^* = ([D^-(w_i, w_j)]_4 + [F_1(w_i)]_4) / h_{2,ij}$, respectively, being $h_{l,ij} = \frac{h_{l,i} + h_{l,j}}{2}$. Some other definitions are possible, as the one proposed in [10].

Theorem 3.1. *The previous numerical scheme exactly preserves the water at rest solutions given by*

$$\vec{u}_{1,i} = 0, \quad \vec{u}_{2,i} = 0, \quad h_{1,i} + h_{2,i} = cst, \quad \frac{1}{|K_i|} \sqrt{\sum_{j \in K_i} \left(\frac{h_{2,j} - h_{2,i}}{\Delta x \eta_{i,j,1} + \Delta y \eta_{i,j,2}} \right)^2} \leq \mu.$$

The proof is similar to the one performed in [9].

4. Numerical tests: submarine collapse of initially cylindrical granular masses. In this section we simulate a set of submarine circular dam-break problems and we also compare them with some existing laboratory data for the case of aerial avalanches. Let us denote by R the radius of the initial granular column and by H_2 its initial height. H_1 designs the initial height of the water layer above the sediment column (See Figure 3). We introduce two aspect ratios : $a_H = H_1/H_2$ and $a_2 = H_2/R$. By scaling the equations as proposed below, we observe that the dimensionless equations only depend on a_H and a_2 and not on the granular mass or on the gravity acceleration g .

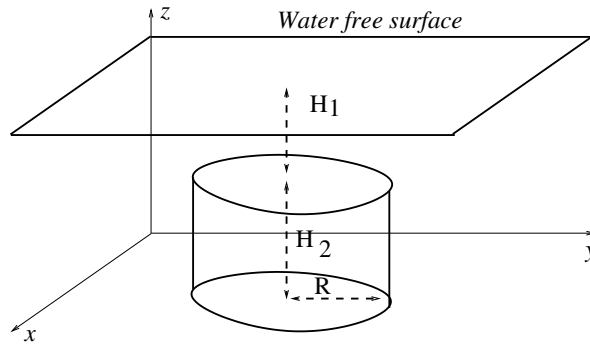


FIGURE 3. Initial condition and notation

The following change of variable is done:

$$(x, y) = (R \tilde{x}, R \tilde{y}), \quad t = \sqrt{\frac{R}{g}} \tilde{t},$$

$$U_l = \sqrt{g H_1} \tilde{U}_l, \quad V_l = \sqrt{g H_1} \tilde{V}_l, \quad h_l = H_1 \tilde{h}_l, \quad l = 1, 2.$$

By omitting the tildes, we obtain the following system

$$\left\{ \begin{array}{l} \sqrt{\frac{a_H}{a_2}} \partial_t (h_1) + a_H \partial_x (h_1 U_1) + a_H \partial_y (h_1 V_1) = 0, \\ \sqrt{\frac{a_H}{a_2}} \partial_t (h_1 U_1) + a_H \partial_x (h_1 U_1^2) + a_H \partial_y (h_1 U_1 V_1) + h_1 \partial_x (a_H h_1 + h_2) = 0 \\ \sqrt{\frac{a_H}{a_2}} \partial_t (h_1 V_1) + a_H \partial_x (h_1 U_1 V_1) + a_H \partial_y (h_1 V_1^2) + h_1 \partial_y (a_H h_1 + h_2) = 0 \\ \frac{1}{\sqrt{a_2}} \partial_t (h_2) + \partial_x (h_2 U_2) + \partial_y (h_2 V_2) = 0, \\ \frac{1}{\sqrt{a_2}} \partial_t (h_2 U_2) + \partial_x (h_2 U_2^2) + \partial_y (h_2 U_2 V_2) + h_2 \partial_x (r a_H h_1 + h_2) = \mathcal{T}_x \\ \frac{1}{\sqrt{a_2}} \partial_t (h_2 V_2) + \partial_x (h_2 U_2 V_2) + \partial_y (h_2 V_2^2) + h_2 \partial_y (r a_H h_1 + h_2) = \mathcal{T}_y \end{array} \right.$$

where

$$\mathcal{T} = -\frac{a_2(1-r)h_2\mu}{\sqrt{U_2^2 + V_2^2}} \begin{pmatrix} U_2 \\ V_2 \end{pmatrix}.$$

and $\mu = \tan \delta$. So, the solutions are mainly governed by the values of a_H , a_2 , r and δ .

In what follows, we initially check that the previous numerical scheme is able to recover the stationary profiles of aerial avalanches. Aerial avalanches (not submerged) can be described here by setting $r = 0$. Next, we will consider fully submerged landslides and we perform some sensitivity analysis with respect to the parameters a_H , a_2 , r and δ .

The initial condition is $\vec{q}_1 = \vec{0}$, $\vec{q}_2 = \vec{0}$,

$$\begin{aligned} h_1(\mathbf{x}, 0) &= a_H a_2 R + a_2 R - h_2(\mathbf{x}, 0), \\ h_2(\mathbf{x}, 0) &= \begin{cases} a_2 R & \text{if } (x - x_0)^2 + (y - y_0)^2 \leq (R)^2, \\ 0 & \text{otherwise.} \end{cases} \end{aligned}$$

We set the domain $[0, 0.6]\text{m} \times [0, 0.6]\text{m}$, the center of the cylinder is $(x_0, y_0) = (0.3\text{m}, 0.3\text{m})$ and $R = 0.0705\text{m}$. The domain is decomposed in 200×200 square finite volumes.

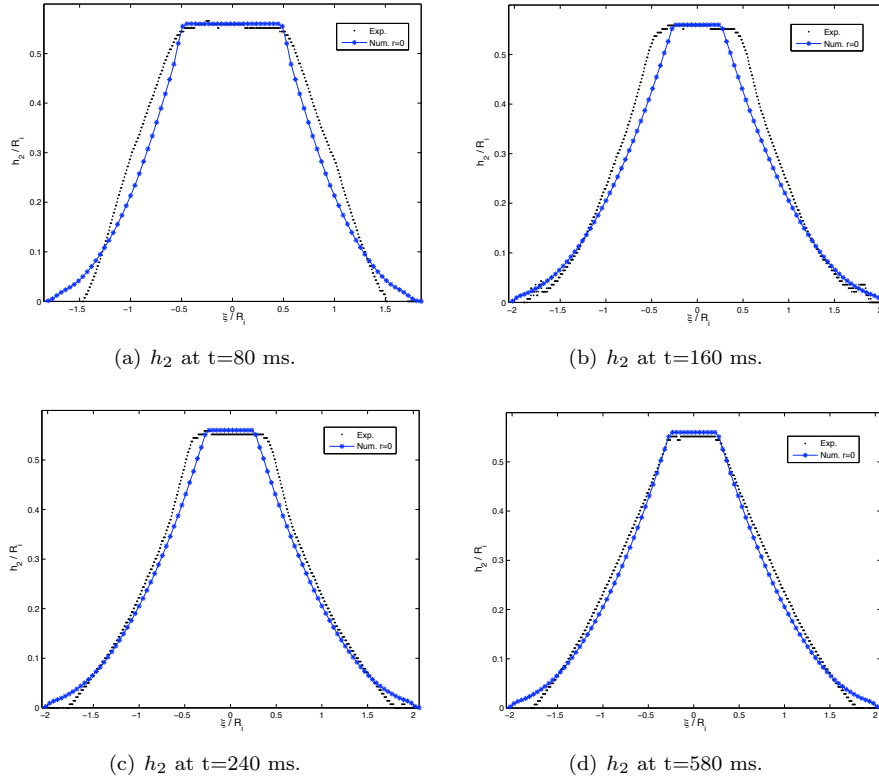
We compare the numerical solutions for $r = 0$, $r = 0.2$, $r = 0.4$, $r = 0.6$ and $r = 0.8$ with laboratory data of dry granular flows, i. e. corresponding to $r = 0$. The case $r = 0.2$ is presented to show the transition between submarine and aerial avalanches. The test is done for $a_2 = 0.56$ as in the experiments (1) in the sub-aerial case and (2) for different values of the relative height $a_H = 1, 2, 10$ to assess the sensitivity of the flow dynamics and generated tsunami to the water depth.

We also denote

$$\eta(\mathbf{x}, t) = h_1(\mathbf{x}, t) + h_2(\mathbf{x}, t) - A_{ref}.$$

where A_{ref} is the reference water surface. For this test $A_{ref} = h_1(\mathbf{x}, 0) + h_2(\mathbf{x}, 0)$.

We begin with the experiments corresponding to $a_2 = 0.56$. First, in Figure 4 the comparison between the experiment with $r = 0$ and experimental data is presented. A good agreement of the numerical results and the laboratory data can be observed.

FIGURE 4. Granular mass profiles. h_2 evolution for $r = 0$.

In Figure 5 a comparison between the evolution of the sediment layer for different values of r is presented, where a_H is set to 1. For other values of a_H , similar behaviour is obtained. The evolution of the submarine avalanche depends on r . For smaller values of r , the final deposit is quickly reached.

In Figure 6 we present the evolution of the front of the avalanche denoted by x_{front} . Figure 6(c) correspond to L_f , the final length of the deposit. We observe that the final length of the avalanche is smaller for bigger values of r and bigger values of a_H . The main difference of the final length between the aerial avalanche (corresponding to $r = 0$) and submarine avalanches corresponds to $r = 0.8$ and $a_H = 10$.

In Figure 7 we present the evolution of x_{front} , for the values $a_H = 1$ and $a_H = 10$. We can observe how, effectively the final deposit is reached previously for smaller values of r , i. e. the propagation time is smaller. The front position is more sensitive to r for $a_H = 1$ than for $a_H = 10$.

In Figure 8 we represent the evolution of $\max_x |\eta(\mathbf{x}, t)|$, for $t = 80, 160, 240$ and 540 ms. We observe that the perturbation of the water surface are bigger from smaller values of r and also smaller values of the aspect ratio a_H . Indeed, the spreading has been shown to be faster for small values of r and the water surface is more sensitive to the granular flow if it is closer to it. For $a_H = 10$ there is almost no perturbation of the water surface, during the submarine avalanche. In Figure

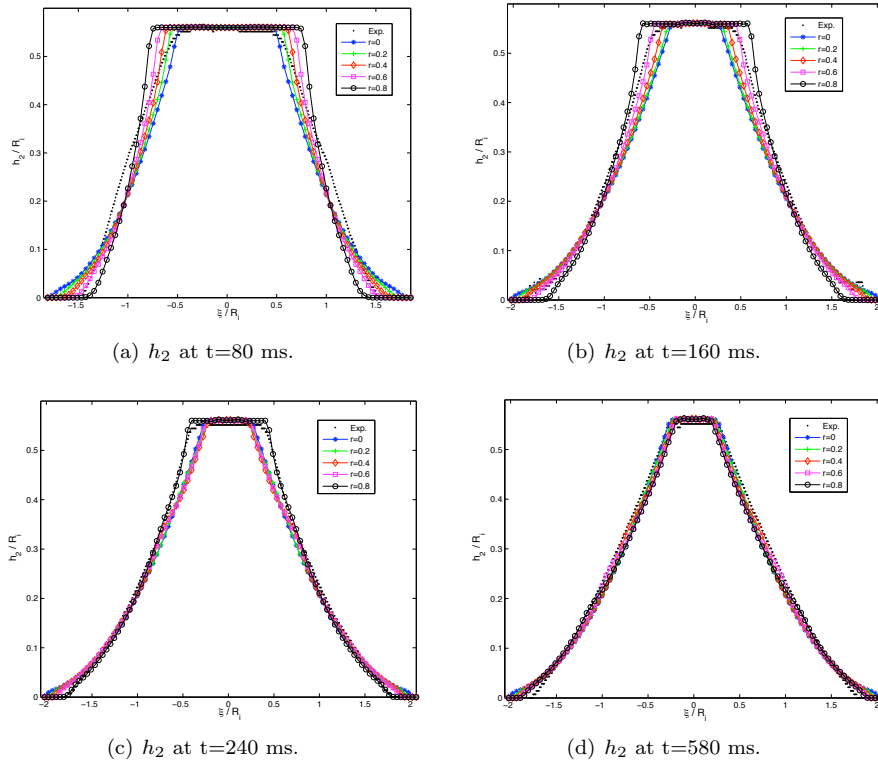


FIGURE 5. Granular mass profiles. h_2 evolution for $a_H = 1$, $r \in \{0, 0.2, 0.4, 0.6, 0.8\}$.

9 the evolution of the water surface for $a_H = 1$ and $a_H = 2$ is presented. We can observe the different behaviour of the water surface, depending on the initial aspect ratios.

In Figure 10 the tridimensional evolution of the sediment avalanche and water surface, for $r = 0.4$ and $a_H = 1$ is presented.

5. Conclusion. In this work we present a preliminary study of the influence of the ratio of densities and the characteristic dimensions of a cylindrical submarine landslide over a flat bottom topography. This is done by considering a 2D generalization of the model presented in [9] where the bottom topography is supposed to be flat. The 2D system is discretized by a first order Riemann solver that results of the combination of the IFCP and HLL Riemann solvers. In particular, the solver reduces to the HLL in wet/dry regions, while the IFCP solver is used in the other regions. Finally, the model has been written in non-dimensional variables in terms of the aspect ratio between the initial height of the avalanche and the initial height of the fluid above the granular mass, and the aspect ratio of the initial sediment mass. The evolution of the maximum amplitude of the free surface and the front position has been studied in terms of the aspect ratios, the ratio of densities r and the friction angle. A comparison with experimental data for the limit case when $r = 0$, corresponding to aerial avalanches has been also presented. We observe that

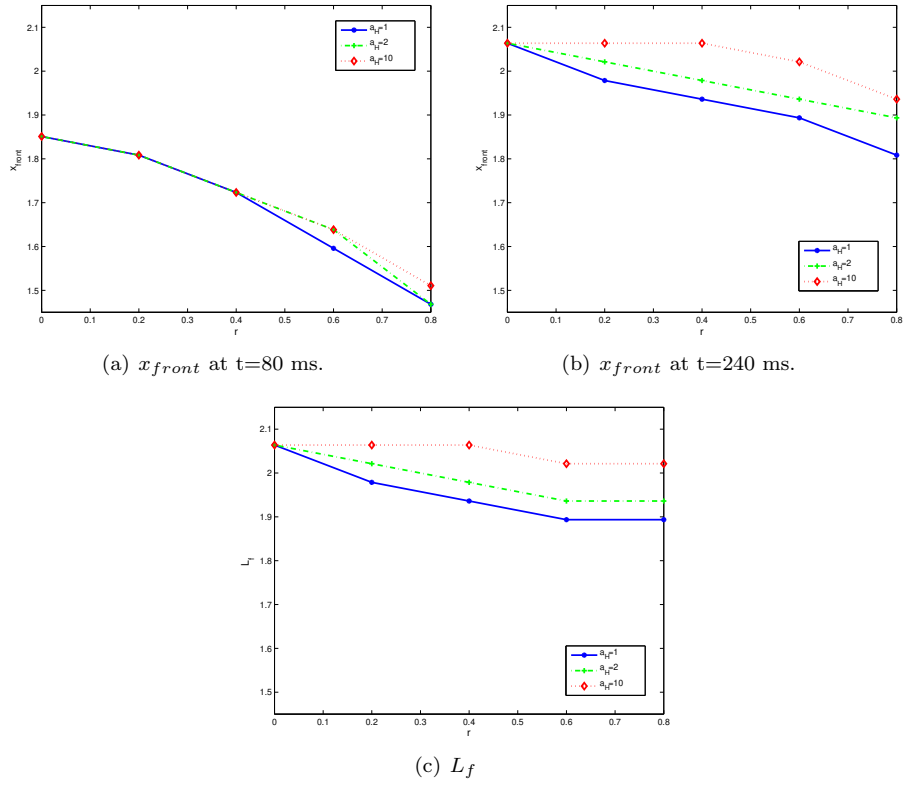


FIGURE 6. x_{front} evolution and L_f for $r \in \{0, 0.2, 0.4, 0.6, 0.8\}$, $a_H \in \{1, 2, 10\}$.

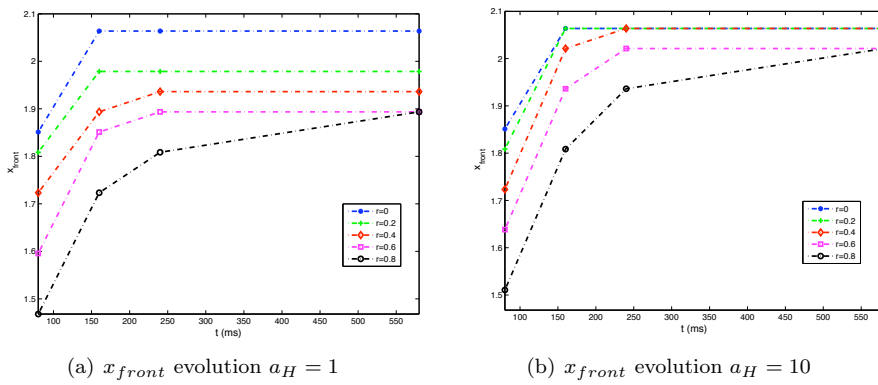


FIGURE 7. x_{front} for $a_H = 1$ and $a_H = 10$ for $r \in \{0, 0.2, 0.4, 0.6, 0.8\}$.

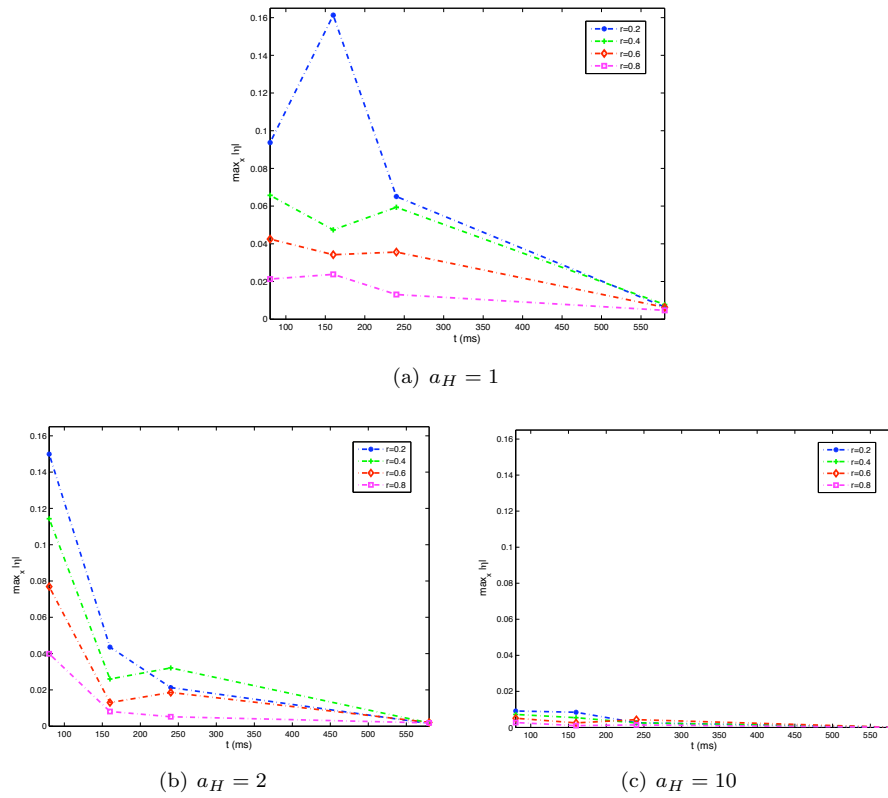


FIGURE 8. $\max_x |\eta|$ for $a_H = 1$, $a_H = 2$ and $a_H = 10$, $r \in \{0.2, 0.4, 0.6, 0.8\}$.

the mass spreading takes more time and lead to smaller runout distance for granular flows of smaller density, leading to a smaller amplitude of the generated water wave. When the granular mass is closer to the water free surface, the runout of the granular flow is smaller but the generated water wave is bigger than when it is 10 times deeper. For intermediate values of the water depth, the behavior is more complex.

REFERENCES

- [1] F. Bouchut, A. Mangeney-Castelnau, B. Perthame, J.P. Vilotte, A new model of Saint Venant and Savage-Hutter type for gravity driven shallow flows. *C.R. Acad. Sci. Paris, Ser I*, **336** (2003), 531–536.
- [2] F. Bouchut, E.D. Fernández-Nieto, A. Mangeney, G. Narbona-Reina. A two-phase two-layer model for fluidized granular flows with dilatancy effects. *Journal of Fluid Mechanics*, **801** (2016), 166–221.
- [3] F. Bouchut, M. Westdickenberg. Gravity driven shallow water model for arbitrary topography. *Comm. Math. Sci.*, **2(3)** (2004), 359–389.
- [4] M. Brunet, L. Moretti, A. Le Friand, A. Mangeney, E. Fernandez-Nieto, F. Bouchut. Numerical simulation of the 30-45 ka debris avalanche flow of Montagne Pelée volcano, Martinique: from volcano flank-collapse to submarine emplacement comparison between measurements and numerical modelling. *Natural Hazards*, **87** (2017), 1189–1222.

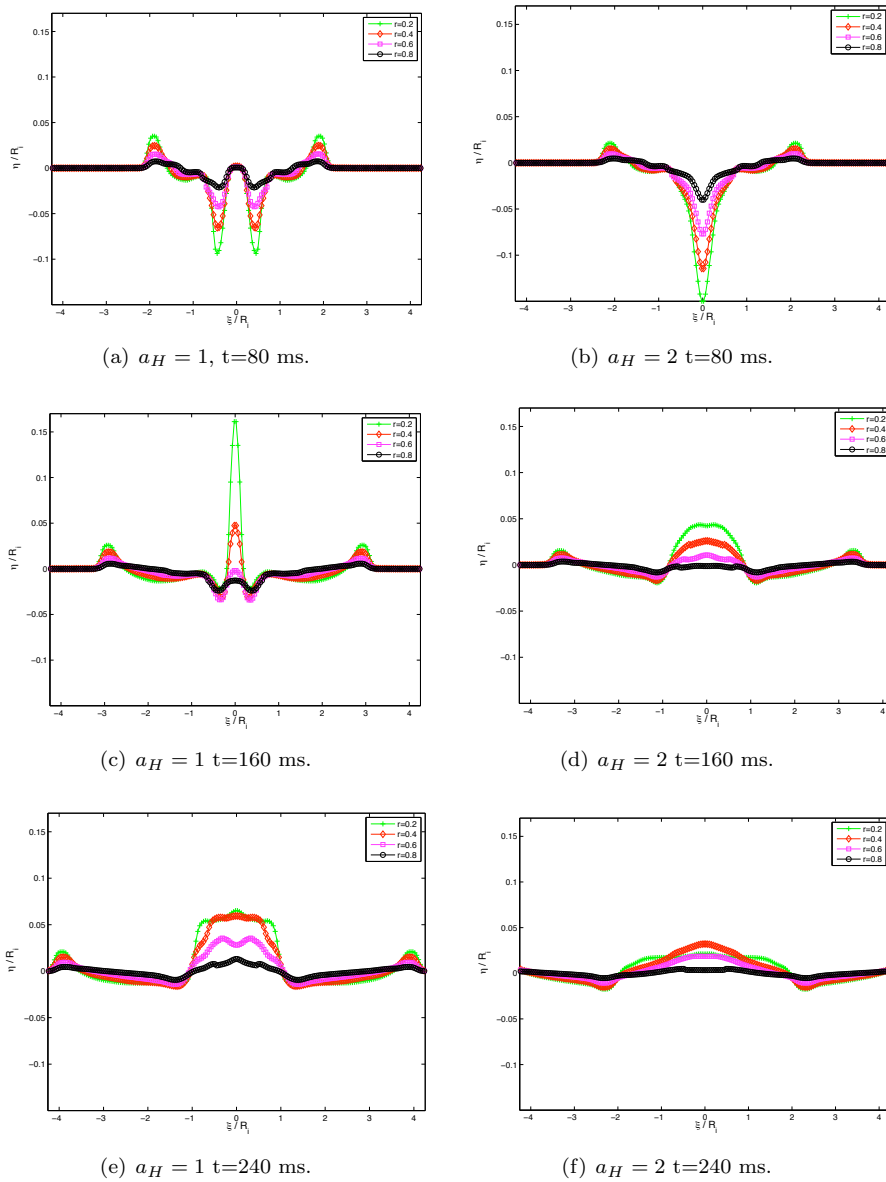
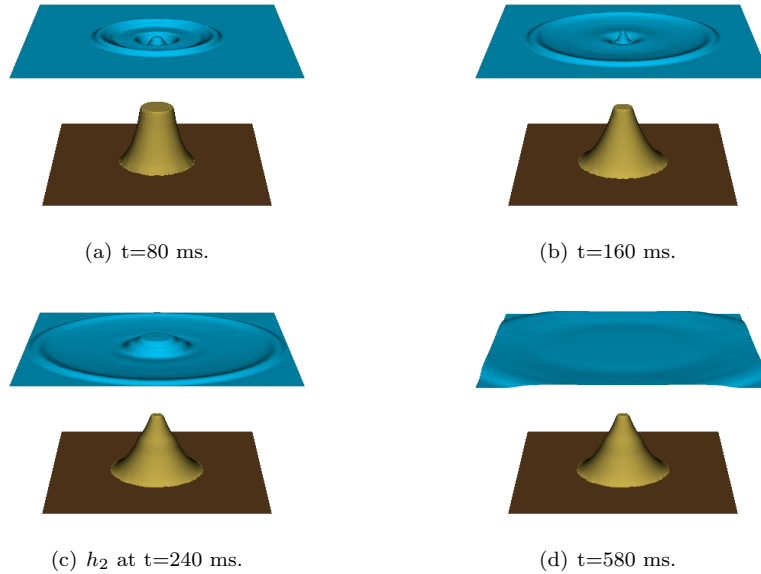


FIGURE 9. Free surface evolution for $a_H = 1$ and $a_H = 2, r \in \{0.2, 0.4, 0.6, 0.8\}$.

[5] M.J. Castro Díaz, T. Chacón Rebollo, E.D. Fernández-Nieto, J.M. González Vida. C. Parés. Well-balanced finite volume schemes for 2D non-homogeneous hyperbolic systems. Application to the dam break of Aznalcóllar. *Comput. Methods Appl. Mech. Engrg.* **197(45-48)** (2008), 3932–3950.

[6] M. J. Castro-Díaz and E. D. Fernández-Nieto. A class of computationally fast first order finite volume solvers: PVM methods. *SIAM Journal on Scientific Computing*, **34(4)** (2012), A2173–A2196.

FIGURE 10. h_2 and surface evolution for $a_H = 1$, $r = 0.4$.

- [7] M.J. Castro, E.D. Fernández-Nieto, A. Ferreiro, J.A. García-Rodríguez, C. Parés. High order extensions of Roe schemes for two-dimensional nonconservative hyperbolic systems. *J. Sci. Comput.* **39**(1) (2009), 67–114.
- [8] G. Dal Maso, P.G. LeFloch, F. Murat. Definition and weak stability of nonconservative products. *J. Math. Pures Appl.* **74** (1995), 483–548.
- [9] E. D. Fernández-Nieto, F. Bouchut, D. Bresch, M.J. Castro, A. Mangeney. A new Savage-Hutter type model for submarine avalanches and generated tsunamis. *J. Comput. Phys.* **227**(16) (2008), 7720–7754.
- [10] E.D. Fernández-Nieto, D. Bresch, J. Monnier. A consistent intermediate wave speed for a well-balanced HLLC solver. *C. R. Math. Acad. Sci. Paris* **346**(13-14) (2008), 795–800.
- [11] E.D. Fernández-Nieto, M.J. Castro-Díaz, C. Parés, C. On an Intermediate Field Capturing Riemann Solver Based on a Parabolic Viscosity Matrix for the Two-Layer Shallow Water System. *Journal of Scientific Computing*, **48**(1) (2011), 117–140.
- [12] E. Godlewski E, P.A. Raviart. Numerical approximation of hyperbolic systems of conservation laws. New York: Springer-Verlag, (1996).
- [13] A. Harten, P. D. Lax, and B. van Leer. On upstream differencing and Godunov-type schemes for hyperbolic conservation laws. *SIAM Review*, **25**(1) (1983), 35–61.
- [14] Lajeunesse, E., A. Mangeney-Castelnau, J. P. Vilotte. Spreading of a granular mass on a horizontal plane. *Phys. Fluids*, **16** (2004), 2371–2381.
- [15] A. Mangeney-Castelnau, J.P. Vilotte, M.O. Bristeau, B. Perthame, F. Bouchut, C. Simeoni, S. Yernini. Numerical modeling of avalanches based on Saint-Venant equations using a kinetic scheme. *J. Geophys. Res.* (2003) 108 (B11), 2527.
- [16] A. Mangeney-Castelnau, F. Bouchut, J. P. Vilotte, E. Lajeunesse, A. Aubertin, M. Pirulli. On the use of Saint Venant equations to simulate the spreading of a granular mass. *J. Geoph. Res.* **110** (2005), B09103.
- [17] A. Mangeney, F. Bouchut, N. Thomas, J.P. Vilotte, M.O. Bristeau, M.O. Numerical modeling of self-channeling granular flows and of their levee-channel deposits. *J. Geophys. Res.* (2007) **112**, F02017.
- [18] S. McDougall, O. Hungr, O. Dynamic modelling of entrainment in rapid landslides. *Can. Geotech. J.* **42** (2005), 1437–1448.

- [19] C. Parés. Numerical methods for nonconservative hyperbolic systems: a theoretical framework. *SIAM J. Numer. Anal.* **44**(1) (2004), 300–321.
- [20] C. Parés, M.J. Castro. On the well-balance property of Roe’s method for nonconservative hyperbolic systems. Applications to shallow-water systems. *ESAIM: M2AN*, **38**(5) (2004), 821–852.
- [21] C. Parés, M.L. Muñoz-Ruiz. On some difficulties of the numerical approximation of non-conservative hyperbolic systems. *Bol. Soc. Esp. Mat. Apl. (SEMA)*, **47** (2009), 23–52.
- [22] M. Pirulli, A. Mangeney. Result of Back-Analysis of the Propagation of Rock Avalanches as a Function of the Assumed Rheology. *Rock Mech. Rock Engng.*, **41**(1) (2008), 59–84.
- [23] O. Pouliquen. Scaling laws in granular flows down rough inclined planes. *Phys. Fluid.* **11** (1999), 542–548.
- [24] S.B. Savage, K. Hutter. The dynamics of avalanches of granular materials from initiation to run-out. *Acta Mech.* **86** (1991) 201–223.
- [25] J.D. Zabsonré, G. Narbona-Reina. Existence of global weak solution for a 2D viscous bilayer Shallow-Water model. *Nonlin. Anal. Real World Appl.* **10**(5) (2009) 2971–2984.
- [26] E.F. Toro. *Shock-Capturing Methods for Free-Surface Shallow Flows*, Wiley, England (2001).

E-mail address: edofer@us.es

E-mail address: castro@anamat.cie.uma.es

E-mail address: mangeney@ipgp.jussieu.fr